REPORT DOCUMENTATION PAGE

Form Approved
OMB No. 0704-0188

1. REPORT DATE *(DD-MM-YYYY)*	2. REPORT TYPE	3. DATES COVERED *(From - To)*
February 2012	Journal Article	

4. TITLE AND SUBTITLE

Experimental and Numerical Analysis of Narrowband Coherent Rayleigh-Brillouin Scattering in Atomic and Molecular Species (Pre Print)

5a. CONTRACT NUMBER

5b. GRANT NUMBER

5c. PROGRAM ELEMENT NUMBER

6. AUTHOR(S)
Barry M. Cornell; Sergey F. Gimelshein; Mikhail N. Schneider; Taylor C. Lilly; and Andrew Ketsdever

5d. PROJECT NUMBER

5f. WORK UNIT NUMBER
Q0G5

7. PERFORMING ORGANIZATION NAME(S) AND ADDRESS(ES)

Air Force Research Laboratory (AFMC)
AFRL/RZSA
10 E. Saturn Blvd.
Edwards AFB CA 93524-7680

8. PERFORMING ORGANIZATION REPORT NUMBER

9. SPONSORING / MONITORING AGENCY NAME(S) AND ADDRESS(ES)

Air Force Research Laboratory (AFMC)
AFRL/RZS
5 Pollux Drive
Edwards AFB CA 93524-7048

10. SPONSOR/MONITOR'S ACRONYM(S)

11. SPONSOR/MONITOR'S NUMBER(S)
AFRL-RZ-ED-JA-2012-044

12. DISTRIBUTION / AVAILABILITY STATEMENT

Approved for public release; distribution unlimited (PA #12126).

13. SUPPLEMENTARY NOTES
For publication in *Optics Express.*

14. ABSTRACT

Coherent Rayleigh-Brillouin scattering (CRBS) lineshapes generated from an all narrow-band pump experiment, a Direct Simulation Monte-Carlo (DSMC) approach, and published simplified models are presented for argon, molecular nitrogen, and methane at 300 & 500 K and 1 atm. The simplified models require uncertain gas properties, such as bulk viscosity, and assume linearization of the kinetic equations from low intensities (<1 x 1015 W/m2) operating in the perturbative regime. DSMC, a statistical approach to the Boltzmann equation, requires only basic gas parameters available in literature and simulates the forcing function from first principles, without assumptions on laser intensity. The narrow band experiments show similar results to broadband experiments and validate the use of DSMC for the prediction of CRBS lineshapes.

15. SUBJECT TERMS

16. SECURITY CLASSIFICATION OF:			17. LIMITATION OF ABSTRACT	18. NUMBER OF PAGES	19a. NAME OF RESPONSIBLE PERSON
					Marcus P. Young
a. REPORT	b. ABSTRACT	c. THIS PAGE	SAR	12	19b. TELEPHONE NUMBER *(include area code)*
Unclassified	**Unclassified**	**Unclassified**			N/A

Experimental and numerical analysis of narrowband Coherent Rayleigh-Brillouin Scattering in atomic and molecular species

Barry M. Cornella,[1] Sergey F. Gimelshein,[1] Mikhail N. Shneider,[2] Taylor C. Lilly,[3,*] and Andrew D. Ketsdever[4]

[1] *ERC Inc., Edwards AFB, CA 93524, USA*
[2] *Department of Mechanical and Aerospace Engineering, Princeton University, Princeton, NJ 08544, USA*
[3] *Department of Mechanical and Aerospace Engineering, University of Colorado Colorado Springs, Colorado Springs, CO 80918, USA*
[4] *Air Force Research Laboratory, Edwards AFB, CA 93524, USA*
[*] tlilly@uccs.edu

Abstract: Coherent Rayleigh-Brillouin scattering (CRBS) lineshapes generated from an all narrow-band pump experiment, a Direct Simulation Monte-Carlo (DSMC) approach, and published simplified models are presented for argon, molecular nitrogen, and methane at 300 & 500 K and 1 atm. The simplified models require uncertain gas properties, such as bulk viscosity, and assume linearization of the kinetic equations from low intensities (<1 x 1015 W/m2) operating in the perturbative regime. DSMC, a statistical approach to the Boltzmann equation, requires only basic gas parameters available in literature and simulates the forcing function from first principles, without assumptions on laser intensity. The narrow band experiments show similar results to broadband experiments and validate the use of DSMC for the prediction of CRBS lineshapes.

OCIS codes: 190.2055 Dynamic gratings, 190.4380 Nonlinear optics, four-wave mixing, 290.5820 Scattering measurements, 290.5830 Scattering, Brillouin, 290.5870 Scattering, Rayleigh, 300.6240 Spectroscopy, coherent transient

References and links

1. R. W. Boyd, *Nonlinear Optics,* (Academic, Boston, 1992).
2. H. J. Metcalf and P. van der Straten, *Laser Cooling and Trapping,* (Springer-Verlag, New York, 1999).
3. J. H. Grinstead and P. F. Barker, "Coherent Rayleigh Scattering," Phys. Rev. Lett., **85**, 1222 (2000).
4. X. Pan, M. N. Shneider, and R. B. Miles, "Coherent Rayleigh-Brillouin Scattering," Phys. Rev. Lett., **89**, 183001 (2002).
5. X. Pan, P. F. Barker, A. V. Meschanov, R. B. Miles and J. H. Grinstead, "Temperature Measurements in Plasmas Using Coherent Rayleigh Scattering," in *Proceedings of the Aerospace Sciences Meeting and Exhibit,* AIAA-2001-0416 (Reno, NV, 2001).
6. X. Pan, P. F. Barker, A. Meschanov, J. H. Grinstead, M. N. Shneider, and R. B. Miles, "Temperature measurements by coherent Rayleigh scattering," Opt. Lett. **27**, 161. (2002).
7. X.P. Pan, M.N. Shneider, R.B. Miles, "Power spectrum of Coherent Rayleigh-Brillouin Scattering in Carbon Dioxide," Phys.Rev. A **71**, 045801 (2005).
8. M. O. Vieitez, E. J. van Duijn, W. Ubachs, A. Meijer, A. S. de Wijn, N. J. Dam, B. Witschas, and W. van de Water, "Coherent and Spontaneous Rayleigh-Brillouin Scattering in Atomic and Molecular Gases and Gas Mixtures," Phys. Rev. A **82**, 043836 (2010).
9. X. Pan, "Coherent Rayleigh-Brillouin Scattering," Princeton University (Ph.D. Thesis, 2003).
10. D. Bruno, M. Capitelli, S. Longo, and P. Minelli, "Monte Carlo Simulation of Light Scattering Spectra in Atomic Gases," Chem. Phys. Lett. **422**, 571 (2006).
11. T. Lilly, S. Gimelshein, A. Ketsdever, and M. Shneider, "Energy Deposition into a Collisional Gas from Optical Lattices Formed in an Optical Cavity," in *Proceedings of the 26th International Symposium on Rarefied Gas Dynamics*, 2008, T. Abe ed. (AIP, New York, 2009), pg. 533.

12. T. Lilly, A. Ketsdever, and S. Gimelshein, "Resonant Laser Manipulation of an Atomic Beam," in *Proceedings of the 27th International Symposium on Rarefied Gas Dynamics,* 2010, D. Levin ed. (AIP, New York, 2011).
13. T. Lilly, "Simulated Nonresonant Pulsed Laser Manipulation of a Nitrogen Flow," Appl. Phys. B **104** (4), 961 (2011).
14. M. N. Shneider and P. F. Barker, "Optical Landau Damping," Phys. Rev. A **71** (5), 053403 (2005).
15. M. N.Shneider, P. F. Barker and S. F. Gimelshein, "Molecular Transport in Pulsed Optical Lattices,"Appl. Phys. A **89** (2), 337-350 (2007).
16. A. Stampanoni-Panariello, D. N. Kozlov, P. P. Radi, and B. Hemmerling, "Gas-Phase Diagnostics by Laser-Induced Gratings I," Appl. Phys. B **81**, 101 (2005).
17. A. Stampanoni-Panariello, D. N. Kozlov, P. P. Radi, and B. Hemmerling, "Gas-Phase Diagnostics by Laser-Induced Gratings II," Appl. Phys. B **81**, 113 (2005).
18. H. Eichler, P. Gunter, and D. Pohl, *Laser-Induced Dynamic Gratings* (Springer-Verlag, Berlin, 1986).
19. X. Pan, M. N. Shneider, and R. B. Miles, "Coherent Rayleigh-Brillouin Scattering in Molecular Gases," Phys. Rev. A **69**, 033814 (2004).
20. H. Bookey, A. Bishop, M. N. Shneider, and P. Barker, "Narrow-Band Coherent Rayleigh Scattering," J. Raman Spectrosc. **37**, 655 (2006).
21. A. Manteghi, N. J. Dam, A. S. Meijer, A. S. de Wijn, and W. van de Water, "Spectral Narrowing in Coherent Rayleigh-Brillouin Scattering," Phys. Rev. Lett. **107**, 173903 (2011).
22. E. Hecht, *Optics* (Addison Wesley, San Francisco, 2002).
23. T. X. Phuoc, "Laser Spark Ignition Experimental Determination of Laser-Induced Breakdown Thresholds of Combustion Gases," Opt. Comm. **175**, 419 (2000).
24. H. T. Bookey, M. N. Shneider, and P. F. Barker, "Spectral Narrowing in Coherent Rayleigh Scattering,"Phys. Rev. Lett. **99**, 133001 (2007).
25. M. S. Ivanov and S. F. Gimelshein, "Current Status and Prospects of the DSMC Modeling of Near-Continuum Flows of Non-Reacting and Reacting Gases," in *Proceedings of the 23rd International Symposium on Rarefied Gas Dynamics* (2003), pp. 339-348.
26. G.A Bird, *Molecular Gas Dynamics and the Direct Simulation of Gas Flows* (Oxford University Press, New York, 1994).
27. M. S. Ivanov, A. V. Kashkovsky, S. F. Gimelshein, G. N. Markelov, Thermophysics and Aeromechanics **4** (3), 251 (1997).
28. C. Borgnakke and P. Larsen, "Statistical Collision Model for Monte Carlo Simulation of Polyatomic Gas Mixture," J. Comput. Phys. **18**, 405 (1975).
29. J.G. Parker, "Rotational and Vibrational Relaxation in Diatomic Gases." *Phys. Fluids* **2**(4), 449 (1959).
30. R. C. Millikan, and D. R. White, "Systematics of Vibrational Relaxation," J. Chem. Phys. **39**(12), 3209 (1966).
31. S. F. Gimelshein, I. D. Boyd, and M. S. Ivanov, "DSMC Modeling of Vibration-Translation Energy Transfer in Hypersonic Rarefied Flows," AIAA Paper 99-3451 (1999).
32. N. E. Gimelshein, D. A. Levin, and S. F. Gimelshein, "Hydroxyl Formation Mechanisms and Models in High-Altitude Hypersonic Flows," AIAA Journal 41(7), 1323 (2003).
33. R. Jansen, S. Gimelshein, M. Zeifman, I. Wysong, and U. Buck, "Nonequilibrium Numerical Model of Homogeneous Condensation in Argon and Water Vapor Expansions," J. Chem. Phys. **132**, 244105 (2010).
34. *CRC Handbook of Chemistry and Physics, 90th ed*., D. R. Lide ed. (CRC, Boca Raton, FL, 2009).
35. G. J. Prangsma, A. H. Alberga, and J. J. M. Beenakker, "Ultrasonic Determination of the Volume Viscosity of N2, CO, CH4 and CD4 Between 77 and 300 K," Physica **64**, 278 (Amsterdam, 1973).
36. G. Emanuel, "Bulk Viscosity of a Dilute Polyatomic Gas," Phys. Fluids A **2**, 2252 (1990).

1. Introduction

Laser-gas interactions within pulsed optical lattices have proven to be a useful tool in gas diagnostics and characterization. Coherent Rayleigh scattering (CRS) and coherent Rayleigh-Brillouin scattering (CRBS) utilize low intensity, relative to breakdown, laser pulses to form a light interference pattern referred to as an optical lattice [1]. This optical potential pattern in turn induces a periodic density perturbation in a gas sample with a periodicity on the order of the laser wavelength [2]. By scattering a probe laser off the density grating formed by the lattice, seen in Fig. 1, the returned signal can be connected spectroscopically to the thermodynamic properties and velocity distribution of the gas sample [3,4]. The necessary

intermediate step is predicting the strength of the density perturbation for a given set of laser and gas parameters.

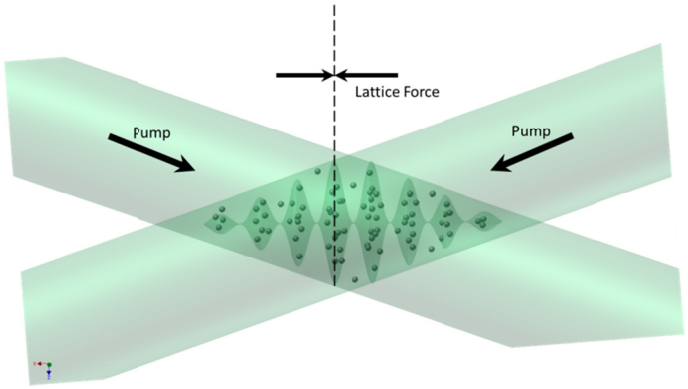

Fig. 1. Schematic of a one-dimensional optical lattice, as formed by a CRBS experiment.

CRBS, as a gas diagnostic technique, has proven its use for yielding information about a gas, such as temperature [5,6] and bulk viscosity [7,8]. Since the pump lasers affect the gas at a kinetic level, the connection between the experimentally obtained lineshape signal returned from the gas density perturbations, and the gas condition, generally requires an approach to solve the Boltzmann equation. Currently, several simplified models are available that do not attempt to solve the Boltzmann equation directly, but use some approximations instead. Depending on the assumptions made, e.g. gas pressure, laser intensity, or species, separate simplified models have been developed for the collisionless [3] or weakly collisional case of CRS and for the collisional case of CRBS [9]. The latter requires further separation based on species, yielding a simplified model for the CRBS lineshape based on the linearized Bhatnagar-Gross-Krook (for atomic species) or Wang-Chang-Uhlenbeck (molecular species) approximations to the 1-D Boltzmann equation. All of the models assume a near equilibrium condition and require bulk viscosity as an input description of the gas.

The present study uses all narrowband lasers for the creation of the gas perturbation in CRBS, creating deeper potential wells than those in broadband experiments. While requiring more tedious scanning of the pump frequencies to create a lineshape, the configuration may ultimately have use in more than purely diagnostic applications. Additionally all narrowband pumps create a monochromatic potential well which can be directly used as a particle forcing function in the numerical approach put forth in this paper. This study also uses a Direct Simulation Monte Carlo (DSMC) approach to predict CRBS lineshapes without making assumptions found in simplified models. Common assumptions include values for hard to find gas parameters, such as bulk viscosity, or the impact of the particle forcing function, such that it is merely perturbative to the equilibrium condition.

The use of a statistical approach (DSMC) to the Boltzmann equation allows for the same information to be predicted for various gas and laser conditions, mainly the magnitude of the induced density perturbation, using a first principles approach to the simulation process. A modified version of the DSMC code, SMILE, was used to calculate the magnitude of the density perturbations caused by non-resonant pulsed optical lattices in a configuration consistent with the performed CRBS experiments. The DSMC method has previously been applied to spontaneous Rayleigh-Brillouin spectra in atomic gases [10], though not previously compared with experiment, and now is applied to scattering in a localized potential field with forced density perturbations (CRBS). SMILE has been used to predict the modification of a neutral gas by several laser configurations [11-13] and is compared directly with an

experiment in this investigation. The line shapes obtained experimentally and numerically are further compared against published atomic and molecular (s6) [9] simplified models.

2. Theoretical Framework

Detailed theory for the effect of an optical lattice on a collisional gas and the scattering of a probe beam off the resulting density perturbation formed by that interaction can be found in [3-4, 14-15]. Background material can be found in closely related fields such as laser induced grating spectroscopy (LIGS) [16,17] or a general book on the topic such as [1,18]. The force acting on a polarizable medium in a non-uniform electric field is given by Boyd [1] as

$$F = -\nabla U = \left(\alpha/2\right)\nabla \mathrm{E}^2 \qquad (1)$$

where α is the directionally averaged static polarizabilty [C m2 V-1] of the particle and E is the electric field [V m-1]. For idealized anti-parallel, coherent, collimated laser pulses, the square of the electric field is calculated as the superposition of two plane waves.

$$\begin{aligned} E^2\left(x,t\right) = {} & E_1^2 cos^2(k_1 x - \omega_1 t) + \\ & E_2^2 cos^2(k_2 x - \omega_2 t) + \\ & E_1 E_2 \begin{bmatrix} cos\left(\left(k_1 - k_2\right)x - \left(\omega_1 - \omega_2\right)t\right) + \\ \cos\left(\left(k_1 + k_2\right)x - \left(\omega_1 + \omega_2\right)\mathrm{t}\right) \end{bmatrix} \end{aligned} \qquad (2)$$

In eq.(2), E1 and E2 represent the electric field amplitudes [V m-1] of laser pulses 1 and 2 respectively, k1 and k2 represent the two pulses' wave numbers [rad m-1], and ω1 and ω2 represent the pulses' angular frequency [rad s-1]. When k_1≈-k_2 and ω_1≈ω_2, the interference term of the field has two components: one with a relatively long spatial and short temporal period and the other with a short spatial and long temporal period. When the gradient of eqn. (2) is taken per eqn. (1), the portion with the long spatial period has a negligible impact. In addition, the fast oscillating terms (⟦cos⟧^2) can be time averaged to a constant value of 1/2. The resulting force acting on a particle within the potential region is given by

$$F = -\nabla U = -\left(\alpha q/2\right)E_1 E_2 \sin\left(qx - \Omega t\right) \qquad (3)$$

where q=k_1-k_2 is the lattice (interference pattern) wave number [rad m-1] and Ω=ω_1-ω_2 is the lattice angular frequency [rad s-1]. Note that q and Ω define the velocity of the lattice, ξ= Ω/q. The sign of Ω defines the direction of ξ. The intensity of the two laser pulses is assumed to have a Gaussian shape in both space (radial) and time which is described by

$$I\left(r,t\right) = I_{\max} \exp\left(-4\ln\left(2\right)\left[\left(t - t_o\right)^2/\tau^2 + r^2/D^2\right]\right) \Rightarrow E_0^2 = 2I/c\epsilon_0 \qquad (4)$$

where Imax is the on-axis peak intensity [W m-2], τ is the laser pulse width (FWHM of I) [s] and D is the laser beam diameter (FWHM of I) [m]. By substituting the laser intensity for the electric field magnitude, eqn. (3) in the axial direction becomes

$$F_x\left(x,r,t\right) = -\alpha q/c\epsilon_0 \sqrt{I_1(r,t)I_2(r,t)}\ \sin(qx - \Omega t) \qquad (5)$$

It should be noted that a gradient in the axial intensity profile caused by the temporal Gaussian shape can be neglected as (2π/q)/(c τfwhm)<<1. This equation gives the force on an individual particle based on its location in space and time relative to the center of the laser pulse's temporal envelope.

With the force on the particles within the gas evaluated, it can be inferred that the periodic nature of the force will induce a local area of higher density at the anti-nodes of the interference pattern [1]. This perturbation in turn causes a periodic structure in the index of refraction of the gas, which is related to its density, effectively creating a grating which will scatter light. Given the CRS/CRBS experimental parameters, such as the angle of the

crossing pumps and the wavelength of the lasers, the scattered light will evolve as a coherent scatter off the grating, increasing the signal significantly over a spontaneous processes [3,4]. It has been shown that the intensity of the returned light in a CRS/CRBS experiment is proportional to the intensity of the probing light and the square of the density perturbations in the gas [3,19]

$$I_{\mathrm{sig}} \propto I_{\mathrm{probe}} \delta\rho^2 \tag{6}$$

For low intensity (perturbative) interactions, it has also been shown that the magnitude of the density perturbation is proportional to the product of the pump laser intensities [3,19]

$$\delta\rho^2 \propto I_{\mathrm{pump1}} I_{\mathrm{pump2}} \tag{7}$$

3. Experimental Setup

CRBS experiment was performed to directly compare with published simplified models and numerical DSMC results. The experimental setup is shown in Fig. 2 and was modeled after previous narrowband CRS setups [20], though used for CRBS lineshapes. It should be noted that this experiment uses all narrowband lasers for CRBS, simplifying the correlation of the two pulses within their coherence distance. The use of all narrowband lasers yields the same results as the use of broadband CRBS pumps, but requires scanning of one of the pump beam's frequency to cover the desired spectral range, instead of the use of an etalon [4] for spectral resolution from a broadband return. Commenting on a recent article which notes "spectral narrowing" when within the coherence distance of the lasers [21], it is understood that if the pump lasers are interfered within their coherence distance, a single interference pattern will form, creating a single frequency density perturbation. Thus, the spectral makeup of the signal, scattered off that single frequency grating, will be close to that of the probe beam. This does not make the configuration useful as a straightforward gas diagnostic technique, the predominant use for CRBS, due to the necessity for long sweeps of the pump laser frequency in order to create a full line shape. However, it does directly relate to the simulated condition of a single frequency optical interference pattern and validates the similarity between narrow- and broadband pumped signals. Lastly, this configuration translates well to future experimental applications requiring deep potential wells, such as gas heating, impossible with broadband pumps.

Two Q-switched, frequency doubled, injection seeded, Nd:YAG lasers, each with ~5 ns pulses, generated the two narrowband pumps (~180 MHz linewidth). The two pump pulses passed through a set of 500 mm focal length lenses and crossed to form the interaction region with a diameter of approximately 100 μm. The crossing angle was approximately 178°. A probe beam was split from pump 1, rotated in polarization orthogonal to the pump beams so not to interfere with the lattice interaction, and separately sent to the interaction region. This configuration required the signal to also be orthogonal in polarization to the pump beams, allowing it to be extracted using a thin film polarizer. The timing of the lasers was controlled by high precision delay generators. Care was taken in matching the path length of the probe to pump 1 and determining the timing of pump 2 to ensure the all three beams arrived at the interaction region simultaneously. The coherence length of the two pulses was approximately 1.6 m based on the speed of sound over the linewidth [22], c/??. For a path length matching to within 0.3 m, the interaction region was well within the coherence length, creating deep monochromatic potential wells. Therefore, the lattice interaction was both coherent and correlated.

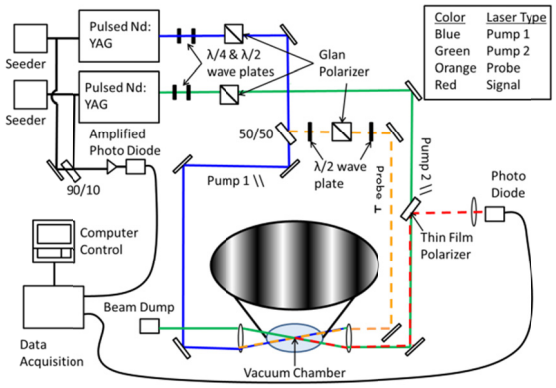

Fig. 2. Schematic of experimental setup.

The phase matching condition is shown in Fig. 3. Because the probe beam and pump 1 were degenerate, the probe beam was set to directly counter-propagate pump 1. This configuration required the scattered signal to propagate counter to pump 2, independent of the frequency difference between the two lasers. The center frequency of pump 2 was varied by a voltage input to the injection seed laser allowing explicit control over the lattice velocity. The frequency was scanned such that the range of the frequency differences varied from 0 to ~5 GHz on the longer runs, at increments of ~15 MHz. Small fractions of each seed laser were interfered and the beat frequency measured on a fast amplified InGaAs photodiode. The measurements were taken on a 7 GHz oscilloscope, yielding a direct measurement of the frequency difference of the pumps at each increment (?f_pump=2?f_seed).

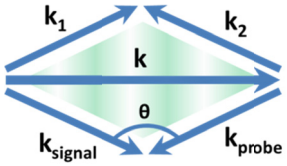

Fig. 3. Phase matching condition for signal backscatter along the path of pump 2.

Three nominal gases were selected for comparison: argon (monatomic), molecular nitrogen (diatomic), and methane (polyatomic). The experiment was performed for gas temperatures of 300 K and 500 K. A small vacuum chamber, which included 532 nm anti-reflective coated windows, was placed at the interaction region and back-filled with the test gas to 1 atm. A diagram of the chamber setup is shown in Fig. 4. Each pump energy was set at approximately 18 mJ, corresponding to an intensity value at the axis at the interaction region (3.0 x 1014 W/m2) well below the breakdown threshold for all test gases [23] and within the small perturbation regime for the lattice-gas interaction [24]. For tests at 500 K, a resistive heater was wrapped around the outside of the chamber. The heater was controlled using a variable transformer and the temperature was measured using a J-type thermocouple. At each frequency point, the scattered beam was detected on a high speed GaAs photodiode and the signal averaged over 100 shots on the oscilloscope. The peak of the averaged signal was then recorded by a LabView interface along with data pertaining to the beat frequency signal and temperature.

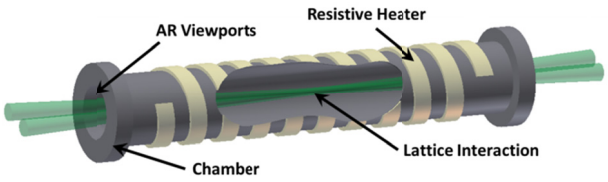

Fig. 4. Diagram of the test chamber.

4. Numerical Setup

The force acting on the molecules directly affects the velocity distribution of the flow, requiring a kinetic approach to model the impact of the laser-species interaction on molecular trajectories. The kinetic code chosen was the DSMC code SMILE. The code was modified to include the non-resonant laser interaction described by eqn. . This modification used a Newtonian integration scheme to approximate the force on a molecule as a temporally and spatially varying acceleration which was considered constant over the duration of a simulation time step. Time steps were therefore reduced such that the species did not traverse appreciable fractions of the laser field or temporal pulse width in one time step. The SMILE code has been broadly applied and experimentally validated, see [25] and the references therein. The variable hard sphere (VHS) model [26] and majorant frequency scheme [27] are employed for modeling molecular collisions. The latter feature was particularly important for maintaining fidelity while reducing the time step to satisfy the laser interaction conditions. The Larsen-Borgnakke model [28] with temperature-dependent rotational and vibrational relaxation numbers is utilized for rotation/vibration-translation energy transfer.

Assuming the validity of eqn. , the numerical simulation package was used to calculate the density perturbation created by the periodic force given by eqn. . As in the experiment, argon, molecular nitrogen, and methane initially at 1 atm and temperatures of 300 K and 500 K were used as the test gases. Beyond the experiment, nitrogen was simulated at a pressure of 5 atm and water vapor was simulated at 1 atm and 400 K. Due to the use of vacuum hardware for the creation of the gas cell, the ability to experimentally increase the gas pressure beyond 1 atm was not feasible. Condensation of water vapor on the anti-reflective windows also prevented water vapor from being experimentally tested. However, previous experimental efforts have validated the use of the simplified models for varying gas pressure [4] and polar species [7]. These two additional scenarios were compared to the simplified models to address the numerical techniques usefulness with varying pressures and polar molecules.

The nominal set of conditions and laser parameters were chosen to match those contained in the experiment. The nominal condition simulated a pair of 532 nm wavelength, 18 mJ, 100 μm (FWHM), 5 ns (FWHM) pulses interacting with each test gas. The simulation domain was modeled axisymmetrically around the optical axis of the two idealized anti-parallel, counter-propagating pulses. The lattice phase velocity in the forcing function described in eqn. (5) was varied in increments of 50 m/s through the range corresponding to the experiment. In order to cover the temporal shape of the pulses, each pulse simulation ran from $-\tau$ to $+\tau$ where τ was assumed to be 5 ns (FWHM). Therefore, the total time for each simulation was 10 ns. With a laser pulse spatial length of approximately 1.5 m, the axial domain boundaries were considered periodic. The radial domain boundary was considered specular and assumed to represent a sufficiently small cross-section at the center of the laser focus that the surrounding volume was equally affected. Also note that in the perturbative regime, there exists a linear relation between the square of the density perturbation and the scattering efficiency [19]. This allows a representative portion of the optical interaction to be simulated and compared with experiment. The domain was nominally 1064 nm tall and 532

nm wide. A diagram of the domain with an overlay of the maximum potential well depth (Tplot=-2U/k) is shown in Fig. 5(a).

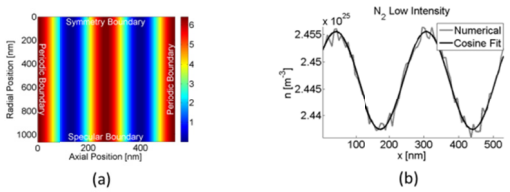

Fig. 5. (a) SMILE simulation domain and maximum potential well depth [K] for an intensity of 3 x 1014 W/m2 and (b) simulated density for a lattice velocity of 450 m/s.

The first step in the simulation procedure was to populate the domain in the baseline ambient configuration with the appropriate gas properties. Flow field properties were sampled every 20th of a run .10th of a pulse width, in order to yield a time dependent evolution of the gas in the simulation domain. With approximately 7,500,000 simulated particles per sample cell, the average statistical error is estimated at approximately 0.1%. The numerical density perturbation was found by a non-linear least squares fit of the axial domain density to a cosine as seen in Fig. 5(b). The magnitude of the cosine fit was used as the magnitude of the density perturbation. As discussed above, the square of the density perturbation is proportional to the magnitude of the scattered signal. The axial domain density perturbation shown in Fig. 5(b) corresponds to the circled point in the numerical/ experimental comparison with a lattice velocity of 450 m/s.

The values of the VHS model [26] parameters used in the DSMC computations are given in Table 1. For methane and nitrogen, vibrational relaxation at temperatures of interest is negligible, and the continuous Larsen-Borgnakke model [28] was used to model vibration-translation and rotation-translation energy transfer, with temperature-dependent relaxation numbers [29,30]. For water, the discrete Larsen-Borgnakke model of rotational and vibrational energies was used [31], with constant rotational and vibrational relaxation numbers Zr=Zv=10 [32]. An atomic model, formulated by Pan et al. [9], was used to predict the CRBS line shape for argon whereas a six moment (s6) model for polyatomic molecules, also formulated by Pan et al. [9], was utilized for comparison with nitrogen and methane. The input gas parameters for the simplified models are given in Table 2, including the y-parameter, defined as [4]

$$y = \frac{8}{3\sqrt{2\pi}} \frac{\rho_0 \sqrt{k_b T_0 / M}}{\eta q} \qquad (7)$$

where kb is Boltzmann's constant and M, ρ0 and T0 are the average gas molecular mass, density and temperature.

Table 1. List of DSMC parameters for each gas species.

Gas	Mass [kg]	Dia. [m]	Visc. Index	T_{ref}	DOF_R	θ_v [K]	Z_R^∞	T*	Source
Ar	6.630 x 10^{-26}	4.170 x 10^{-10}	0.310	273	-	-	-	-	26
CH_4	2.656 x 10^{-26}	4.830 x 10^{-10}	0.340	273	3	2360	15.0	100.0	26
N_2	4.650 x 10^{-26}	4.170 x 10^{-10}	0.240	273	2	3371	23.5	91.0	26
H_2O	2.990 x 10^{-26}	6.200 x 10^{-10}	0.500	273	3	-	10.0	10.0	33

Table 2. List of gas parameters for simplified models.

Gas	T [K]	P [atm]	y	η [Pa s]	η_b/η	k [W/mK]	c_{int}	Source
Ar	300	1	0.46	22.74 x 10^{-6}	-	17.84 x 10^{-3}	-	34,9
Ar	500	1	0.23	34.08 x 10^{-6}	-	26.73 x 10^{-3}	-	34,9
CH_4	300	1	0.70	11.13 x 10^{-6}	2.16	34.19 x 10^{-3}	3/2	34,35,7
CH_4	500	1	0.35	16.92 x 10^{-6}	2.16	68.34 x 10^{-3}	3/2	34,35,7
N_2	300	1	0.57	17.89 x 10^{-6}	0.73	25.97 x 10^{-3}	1	34,9,35,36
N_2	500	1	0.30	26.06 x 10^{-6}	0.73	39.04 x 10^{-3}	1	34,9,35,36
N_2	300	5	2.85	17.89 x 10^{-6}	0.73	25.97 x 10^{-3}	1	34,9,35,36
H_2O	400	1	0.62	11.41 x 10^{-6}	1000	19.76 x 10^{-3}	3/2	34

5. Results and Discussion

The results for the CRBS experimental runs and numerical simulations for argon, molecular nitrogen, and methane at 300 K are shown in Fig. 6. While the magnitude of the density perturbation is not directly measured by the experimental setup, the relative change in the perturbation (squared) is characterized by a corresponding change in signal intensity as described in Eq. (7). The maxima to the experimentally recorded averaged scattered signal are compared to the numerically simulated density perturbations (squared). Each set of results was normalized such that the lineshape trend at 0 m/s was unity. Comparison of the results obtained in this investigation with previously validated simplified models provides verification of both the presented numerical method as well as the narrowband experimental technique.

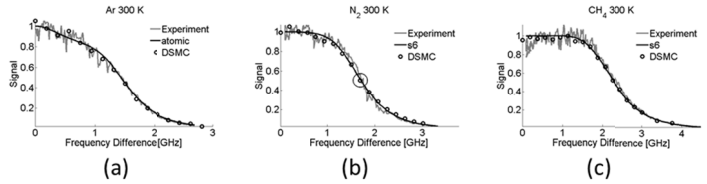

Fig. 6. Comparison of low intensity CRBS line shapes for Ar, N2, and CH4 at 300 K.

Signal in Fig. 6 is shown versus the frequency difference of the two pump beams. For 532 nm pump lasers, the conversion from frequency difference between the pumps to the velocity of the lattice is approximatley 0.38 GHz per 100 m/s. Because the CRBS scheme operates in the perturbative regime, the expected width of the line shape curve (half width half maximum) is on the order of, and should vary with, the mean thermal speed of each species as indicated by the simplified models. Shown in Fig. 6, the numerical results, DSMC, compare favorably to experimental results as well as simplified models for all three gases. Scatter in the experimental data arises from laser pointing instabilities both space and time. In particular, spatial movement due to the frequency locking control loop in each pump cavity and seed laser was occasionally observed to cause fluctuations in signal intensity, similar to those shown in Fig. 6, at various frequency points. However, Fig. 6 reflects that the prominent features, such as overall shape and linewidth, are retained in the experimental data within the scatter. Likewise, the numerical results also capture the general features of the lineshape for each gas within the simulation error.

Using the same gas dynamic parameters in Fig. 6, the simplified model was applied to all three gases at an elevated temperature and compared to results from the numerical simulations and the experiment. Fig. 7 shows the CRBS results at 500 K. Since the CRBS line shape in

the perturbative regime is dictated by collisional gas dynamic phenomena, it follows that the line shape width increases with the square root of temperature which can be seen in all three cases of Fig. 7. Again, the experimental and numerical results compare favorably to the predicted simplified model. For a given lattice potential well depth (intensity), less of the gas is affected as the velocity distribution broadens. Thus, as the temperature of the gas increases, the magnitude of density perturbation created by the lattice decreases for the same pump intensities. Consequently, an increase in relative experimental data scatter occurs due to an overall decrease in signal intensity. As a result, the fluctuations in the higher temperature experimental data set are more pronounced. The error associated with determining the density perturbation in the numerical simulations also increases with temperature due to the decrease in signal to noise ratio. However, as was the case for the lower temperature data sets, both the experimental and numerical results were able to capture both the general line shape as well quantifiably determine a line width.

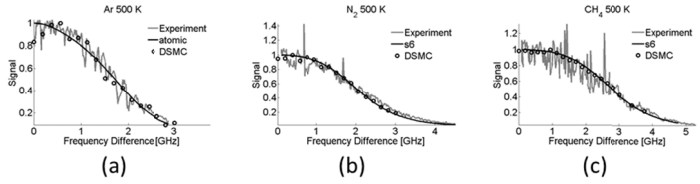

Fig. 7. Comparison of low intensity CRBS line shapes for Ar, N2, and CH4 at 500 K.

DSMC simulations were further applied to two additional scenarios: varying pressure and a polar molecule. Fig. 8(a) shows the comparison of the DSMC numerical predictions for the CRBS line at 1 atm (left) and 5 atm (right) with the line shape predicted by [9]. Both curves are normalized such that the maxima are unity. As shown in Fig. 8(a), Brillouin peaks become much more prominent at higher pressures than at 1 atm and occur at lattice velocities on the order of the speed of sound [4]. The DSMC predictions accurately predict the location of the Brillouin peaks as well as the magnitude (~150% larger than the center Rayleigh peak) for nitrogen at 5 atm. Fig. 8(b) shows the comparison of DSMC simulations to predicted line shape for water vapor at 400 K. A ratio of bulk viscosity to shear viscosity was assumed to be 1000 in the simplified model due to a lack of readily available published data on the value. Fig. 8(c) shows several simplified model lines, using various bulk/shear ratios to show the possibility of using the DSMC to find the bulk viscosity for a gas with well understood internal degrees of freedom. Fig. 8 illustrates that the proposed numerical simulation method can be applied to predicting CRBS spectra for varying pressures as well as for naturally polar species, assuming the permanent dipole moment is less influential than the induced moment for this application.

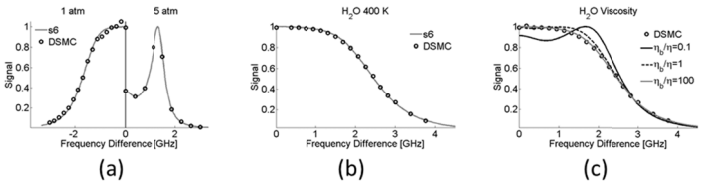

Fig. 7. Comparison of numerical and simplified results for (a) varying N2 pressure, (b) water vapor using s6 & ηb/η=1000, and (c) water vapor using s6 & various ηb/η.

6. Conclusion

The experimental CRBS technique presented in this investigation follows the spirit of previous methods, while using narrowband pumps. A kinetic numerical simulation technique,

DSMC, was applied with laser and gas parameters that directly coincide with the presented experiment. Both the experiment and numerical simulations operated in the low intensity (perturbative) regime allowing comparison with the simplified models which are based on linear approximations to the 1-D Boltzmann equation. It can be assumed for dilute gases that the change in index of refraction, and therefore scattered light, varies with the square of the density perturbation formed by an optical dipole force. Thus, the density perturbation obtained from the simulations was taken as a measurement of the CRBS signal. It has been shown that a DSMC simulation technique can adequately capture the lineshapes of a CRBS experiment. Good agreement was shown for monatomic species as well as diatomic and polyatomic species where internal energies have an influence on the overall lineshape. At elevated temperatures, an expected broadening of the power spectra was shown and verified. Furthermore, DSMC was matched with the experimentally verified simplified models for varying pressure and the use of polar gas species. While current simplified models have adequately predicted CRS and CRBS line shapes for a wide variety of cases, multiple models are required to encompass all scenarios. Utilizing a DSMC approach for modeling CRBS lineshapes has the advantage of broad applicability over a wide variety of scenarios in the perturbative regime, but also the potential ability to determine CRBS line shapes beyond the perturbative regime as no assumption on the forcing function has been made. One such scenario in the perturbative regime is the calculation of line shapes in gas mixtures, for which no simplified model has been formulated.

This work was supported by the Air Force Office of Scientific Research (AFOSR). The authors would like to thank Dr. Mitat Birkan (AFOSR/RSA) for his support of numerical efforts and Dr. Tatjana Curcic (AFOSR/RSE) for her support of experimental efforts. This work was also supported, in part, by a grant of computer time from the DOD High Performance Computing Modernization Program at the U.S. Army Engineer Research and Development Center DoD Supercomputing Resource Center (ERDC DSRC).